Харківський національний університет імені В.Н. Каразіна
Факультет математики і інформатики
Кафедра прикладної математики

Кваліфікаційна робота

рівень: ***магістр***

на тему ***«Чисельне моделювання фокусування електромагнітних хвиль дискретною лінзою Люнебурга з графеновим елементом за допомогою збіжного алгоритму»***

Виконав: студентка групи МП62 II курсу (другий магістерський рівень), спеціальності 113 “Прикладна математика” освітньо-професійної програми “Прикладна математика”
Міхайлікова І.О.

Керівник: канд. фіз.-мат. наук, доц., доцент кафедри прикладної математики
Стєпанова К.В.

Рецензент: Науковий співробітник лаб. мікро- та нанооптики ІРЕ НАН України, доктор філософії
Герасимова Д.

Харків — 2024 рік

V. N. Karazin Kharkiv National University
Faculty of Mathematics and Computer Science
Department of Applied Mathematics

Master thesis

on the topic of ***«Numerical modelling of electromagnetic wave focusing by a graphene-assisted discrete Luneburg lens using a convergent algorithm»***

Author: student of AM62 group of II year
(Master level),
speciality 113
"Applied Mathematics"
educational and professional
program
"Applied Mathematics"
Iryna Mikhailkova

Supervisor: Ph.D. in mathematics,
Associate professor
School of Mathematics
and Computer Sciences
specialties Applied Mathematics
Kateryna Stiepanova

Reviewer: Scientist at Laboratory
of Micro and Nanooptics
Usikov's IRE NAS Ukraine,
Ph.D.
Dariia Herasymova

Kharkiv — 2024

Abstracts

Міхайлікова Ірина Олегівна

Чисельне моделювання фокусування електромагнітних хвиль дискретною лінзою Люнебурга з графеновим елементом за допомогою збіжного алгоритму.

Ми розглядаємо характеристики фокусування, розсіювання та поглинання плоскої хвилі та точкового джерела багатошарової циліндричної лінзи Люнебурга, частково вкритої конформною стрічкою графену, у випадку H-поляризації. Кутова ширина стрічки та розташування на поверхні є довільною, а її поверхневий імпеданс характеризується за допомогою квантово-фізичного формалізму Кубо. Ми використовуємо математично точну повнохвильову аналітичну техніку регуляризації, яка базується на інверсії статичної частини задачі. Це гарантує збіжність отриманого числового алгоритму. Ми обчислюємо здатність фокусування мікролінзи як функцію частоти в широкому діапазоні до 30 THz. Цей аналіз показує, що графенова стрічка, розміщена у фокальній зоні лінзи Люнебурга, покращує її здатність до фокусування на певній резонансній частоті, що відповідає плазмонній моді стрічки.

Ключові слова: лінза Люнебурга, графенова стрічка, багатошаровий діелектричний циліндр, метод аналітичної регуляризації.

Mikhailikova Iryna

Numerical modelling of electromagnetic wave focusing by a graphene-assisted discrete Luneburg lens using a convergent algorithm

We examine the focusing, scattering, and absorption characteristics of a plane wave and point source incident on a multilayer cylindrical Luneburg lens partially covered with a conformal graphene strip in the case of H-polarization. The angular width of the strip is arbitrary and can vary, and its surface impedance is characterized using the quantum-physical formalism of Kubo theory. We employ a mathematically precise full-wave analytical regularization technique based on the inversion of the static part of the problem. This ensures the convergence of the resulting numerical algorithm. We calculate the focusing ability of the microlens as a function of frequency over a wide range up to 30 THz. This analysis shows that the graphene strip placed in the focal region of the Luneburg lens enhances its focusing ability at a specific resonant frequency, proportional to Q-factor of the plasmon mode of the strip.

Key words: Luneburg Lens, graphene strip, layered dielectric cylinder, method of analytical regularization.

Contents

Introduction

Most of the results obtained during this research have been already published in [1] or presented on conference papers [2], [3], [4], [5], [6], [7], [8]. This thesis was largely conducted under the supervision of Professor Sergii V. Dukhopelnykov, whose valuable guidance and support contributed significantly to achieving the research objectives.

The Luneburg lens (LL) is a spherical or circular cylindrical dielectric lens with a radius R_M and relative dielectric permittivity that depends on the radial coordinate r as $\varepsilon(r) = 2 - (r/R_M)^2$. At the lens surface, the permittivity value equals 1. In the geometrical optics (GO) approximation, such a lens has its focal point precisely on its outer surface [10]. In a realistic scenario, an LL has a finite size and is discrete, for instance, concentrically layered [12], with the outer layer of the lens exhibiting a non-negligible contrast with the surrounding medium. When illuminated by plane waves, such lenses do not produce focal points but rather finite-sized focal regions, which shrink to the half-wavelength limit as the lens size increases. The focusing ability of the lens can be evaluated as the maximum field magnitude (normalized to the amplitude of the plane wave) and grows proportionally to kR_M, where k is the wavenumber. Note that in practical systems, the focusing ability deteriorates whenever the frequency coincides with a high-Q whispering-gallery mode of the outer layer of the lens. To shift these frequencies out of the operational range, the lens must be optically large and have a dielectric permittivity of the outer layer close to 1.

Without increasing the size, it is possible to enhance the focusing ability of a quasi-optical antenna using subwavelength resonant elements placed

in the focal region. Recently, this possibility was demonstrated in [20] for a simple dielectric lens antenna in the form of a uniform circular dielectric rod decorated with a conformal graphene strip. The observed improvement is attributed to the interaction between GO focusing, known as the "electromagnetic jet effect" [21], [15], and the plasmonic mode resonances of the graphene strip, provided the latter is located in the focal region.

Indeed, in the case of H-polarization, the graphene strip can support transverse plasmon modes with low natural frequencies. Both the frequencies and corresponding Q-factors can be controlled via the chemical potential of graphene and the electron relaxation time, as predicted by the quantum-physics Kubo theory [16].

Notably, plasmonic modes of dielectric scatterers with graphene elements are an active area of research today [22], [19], [18], [23]. These studies show that such composite scatterers are complex open resonators that support both dielectric modes and plasmonic modes of the graphene elements.

However, it should be noted that the focusing ability of a layered LL and the potential improvement using resonant graphene elements have not yet been studied. On the other hand, the ability of an LL to collimate the main beam of the radiation pattern when fed by a localized source placed on the lens surface was the main focus of study in [12]. For this reason, LL-based antennas are primarily known for their high directivity.

Nevertheless, another important application of an LL is its use as a cross-section amplifier for backscattering (monostatic radar). In such applications, a discrete LL is equipped with a conformal metallic (modeled as perfectly electrically conducting, PEC) "cap" [24], [25]. Unlike the more common rectangular metallic reflector, such a radar target exhibits high reflectivity over a wide range of incident angles.

Replacing the PEC reflector with a graphene one, which supports plasmonic modes, still results in enhanced scattering [5]. Furthermore, since graphene has losses, this configuration demonstrates increased absorption, particularly at the plasmon resonance frequency [6].

The main challenge in accurate full-wave modeling of such a composite scatterer, like an LL with a conformal graphene strip, lies in the fact that the lens has a quasi-optical size, while the width of the graphene strip, to resonate at the lowest plasmon mode, must be deeply subwavelength. For reliable analysis, more efficient, i.e., faster and more precise numerical methods are required than conventional numerical approximations and commercial codes. Based on these considerations, we analyze the scattering from a circular layered dielectric rod with a conformal graphene strip placed on its outer surface using a code based on the method of analytical regularization (MAR) [26], capable of overcoming the above-mentioned difficulties and ensuring guaranteed convergence.

In his famous book [10], Luneburg demonstrated optically efficient use of lenses of cylindrical or spherical shape that have the relative dielectric permittivity depending on the radius as follows: . Hence, it is 2 in the center and 1 at the lens surface. Such lenses are commonly referred to as Luneburg lenses (LL). As shown in the geometrical optics (GO) approximation [10], the largest value of the field amplitude, i.e. the focus, appears at the outer boundary of the continuous-epsilon LL. In the real-life situations, LLs are finite in size and discrete, for instance, concentrically layered [11], [12], [13], [14]. When illuminated with the plane-waves, realistic lenses do not have GO-like focal points. Instead, they display finite-size focal areas of elongated shape, frequently called "electromagnetic jets." If the lens optical size gets larger, these finite focal areas shrink to the half-wavelength limit.

In the emission regime, one of the main antenna characteristics is its directivity. For any finite-size lens, the directivity is known to grow linearly with its electrical or optical size, in terms of the working wavelength. Well-known side effect of making LL layered instead of continuous-epsilon is the appearance of the high-Q periodic whispering-gallery mode (WGM) resonances at high frequencies. Caused by finite optical contrast between the outer layer and the free space, these resonances spoil the LL directivity [12]. To shift WGMs off the operational range, a layered lens should have the outer layer permittivity as close to 1 as possible.

In the reception regime, the main characteristic of a quasioptical antennas is its focusing ability (FA). A chance to raise FA appears with the aid of the resonance elements, of sub-wavelength size with respect to the free-space wavelength, placed into the focal area. Recently, this opportunity has been demonstrated in [15] for the uniform circular dielectric rod and for layered LL [1] decorated with a conformal graphene strip. Indeed, in the case of the H (TE) polarization, the strip of graphene supports the transversal plasmon modes with low natural frequencies and moderate Q-factors. As graphene's conductivity depends on its chemical potential and electron relaxation time (see the quantum-physics Kubo theory [16]), the plasmon-mode characteristics are electrically tunable, that is attractive for applications. Due to the tunability, plasmon modes of dielectric scatterers with graphene elements are actively studied today [17], [18], [19].

In [1], the focusing ability of the Luneburg lens and the influence of a graphene strip located in the focal region of this lens in the reception regime, i.e. in the case of a plane wave incidence, were investigated. This study showed higher efficiency of the lens compared to a simple dielectric rod.

Therefore, it is interesting to study the effect of graphene strip in the

reciprocal situation of the layered LL, fed by a line-current source. Note that such effect has been previously studied for a uniform dielectric rod with a graphene strip excited by a line source [15].

The accurate full-wave modeling of such a composite scatterer as quasi-optical size LL with deeply sub-wavelength conformal strip of graphene is a true challenge. For a trusted analysis, such a lens requires more efficient, i.e. faster and more accurate, computational techniques than conventional numerical approximations and commercial codes. Therefore, we use the code based on the hypersingular integral equation (HIE) discretized with the Nystrom method [15]. Such a technique is completely grounded mathematically and its convergence is guaranteed by the proven theorems. As filling in the final matrix equation does not involve any numerical integrations, it is very fast and provides the accuracy, controlled by the order of discretization.

Dissemination of results. The results of the work were presented and discussed at the following international conferences and symposia:

- IEEE International Conferences on Electronics and Nanotechnologies (ELNANO), Kyiv (2022);
- European Microwave Conferences (EuMC): Milan (2022), Berlin (2023), Paris (2024);
- European Conferences on Antennas and Propagation (EuCAP), Florence (2023), Glasgow (2024);
- IEEE Ukrainian Microwave Week (UkrMW), Kharkiv (2022);
- International Symposium IEEE Antennas and Propagation (AP-S), Florence, (2024).

Publications. The results of research have been published in 9 refereed papers indexed in Scopus, including 1 paper in international journals [1] and

8 papers in the proceedings of international conferences [2] - [9].

The research within this thesis has been recognized by the IEEE Antennas and Propagation Society and the IEEE Photonics Society.

Chapter 1

Geometry and problem formulation

(a) (b)

Figure 1.1: Cross sections of the bare discrete M-layer concentric Luneburg lens decorated with a conformal strip of graphene illuminated by the plane wave (a) and excited by the-point source (b). The strip is shown as a black arc centered at $\phi = 0$.

1.1. Case of a plane wave

Let us consider the case of a plane H-polarized monochromatic wave ($e^{-i\omega t}$) incident on a circular dielectric rod that models a Luneburg lens and is partially covered with a graphene strip. Cylindrical coordinates (r, ϕ, z) are introduced, where the z-axis coincides with the cylinder's axis. The cylinder's radius is denoted as R, and the angular width of the graphene strip is 2δ. Additionally, the gap width is denoted as $2\theta = 2\pi - 2\delta$.

In the case of H-polarization, the electromagnetic field consists of the following components: magnetic $(0, 0, H_z)$ and electric $(E_r, E_\phi, 0)$. Here, R_p and ε_p represent the outer radius and relative dielectric permittivity of the p-th layer, where $p = 1, \ldots, M$. The angular width of the graphene strip is

2δ, while its physical width in cross-section is $L = 2\delta R_M$. Consequently, the gap has an angular width of 2θ.

The black arrow in Fig. 1.1 indicates the propagation direction of the plane wave, while ϕ_0 denotes the incidence angle measured relative to the x-axis.

The following two-dimensional wave-scattering problem is posed: we aim to find the function that satisfies the given conditions.

(i) the Helmholtz equation in the domain bounded by the circles of radii R_j and R_{j+1}, $j = 1, 2, ..., M + 1$ i.e.,

$$\Delta H_z^{(j)}(r, \phi) + (k_j)^2 H_z^{(j)}(r, \phi) = 0 \tag{1.1}$$

with the piecewise wavenumber k_j

$$k_j = (\frac{\omega}{c})\sqrt{\varepsilon_j} = k\alpha_j \tag{1.2}$$

(ii) the dual conditions at $r = R_M$, on the arc with graphene covering $L = \{r = R_M, |\phi| \leq \delta\}$:

$$E_\phi^{(M)} + E_\phi^{(M+1)} = 2ZZ_0(H_z^{(M)} - H_z^{(M+1)}), E_\phi^{(M)} = E_\phi^{(M+1)} \tag{1.3}$$

and on the arc without graphene $S = \{r = R_M, |\phi| \geq \delta\}$:

$$H_z^{(M)} = H_z^{(M+1)}, E_\phi^{(M)} = E_\phi^{(M+1)} \tag{1.4}$$

where M+1 represents the region beyond the lens,

(iii) the tangential components continuity conditions at $r = R_p$, $p = 1, 2, ..., M - 1$,

(iv) the Sommerfeld radiation condition at infinity,

(v) the local power finiteness condition. As known, these conditions guar-

antee the uniqueness of the boundary-value problem solution for all real-valued k.

$$E_{\phi}^{(j)} = -\frac{Z_0}{ik\varepsilon_j}\frac{\partial}{\partial r}H_z^{(j)} \tag{1.5}$$

The incident plane wave can be represented through angular Fourier series:

$$H_z^{inc} = e^{ikx} = e^{ikr\cos\phi} = \sum_{n=-\infty}^{\infty} i^n J_n(kr)e^{in\phi} \tag{1.6}$$

We will look for the total field, which can also be represented through an angular Fourier series in the following form:

$$H_z = \begin{cases} H_z^{(M+1)} + H_z^{inc}, & r \geq R_M \\ H_z^{(j)}, & R_{j-1} < r < R_j, 1 < j < M \\ H_z^{(1)} & r < R_1 \end{cases} \tag{1.7}$$

where $H_z^{(M+1)}$ is the field in the domain outside the lens, $r \geq R_M$

$$H_z^{(M+1)} = \sum_{n=-\infty}^{\infty} d_n H_n(k_{M+1}r)e^{in\phi}/H_n'(k_{M+1}R_M), \tag{1.8}$$

and $H_z^{(1)}$ is the field in the central domain of the lens, $r < R_1$

$$H_z^{(1)} = \sum_{n=-\infty}^{\infty} c_n J_n(k_1 r)e^{in\phi}/J_n'(k_1 R_1), \tag{1.9}$$

and $H_z^{(p)}$ is the field in the layer domain, $R_{p-1} < r < R_p$, $p = 2, ..., M$

$$H_z^{(p)} = \sum_{n=-\infty}^{\infty} [a_n^p J_n(k_p r)/J_n'(k_p R_p) + b_n^p H_n(k_p r)/H_n'(k_p R_p)]e^{in\phi}. \tag{1.10}$$

Based on the continuity condition at the boundary, the following formula

is obtained:

$$\begin{cases} -b_n^2 L_n^2 = c_n G_n^1 \\ a_n^2 K_n^2 = c_n \Gamma_n^1 \end{cases} \tag{1.11}$$

and this system results from the boundary condition between the layers:

$$\begin{cases} a_n^p G_n^p + b_n^p S_n^p = -b_n^{p+1} L_n^{p+1} \\ a_n^p \Gamma_n^p + b_n^p D_n^p = a_n^{p+1} K_n^{p+1} \end{cases} \tag{1.12}$$

where a_n^p, b_n^p, c_n^p, d_n^p are the unknown coefficients that we need to determine. And L_n^p, K_n^p, Γ_n^p, S_n^p, D_n^p, G_n^p can be represented as follows:

$$L_n^p = 2i(\pi k R_{p-1} J_n'(\alpha k_p R_{p-1}) H_n'(k\alpha_p R_p))^{-1} \tag{1.13}$$

$$K_n^p = 2i(\pi k R_{p-1} J_n'(k\alpha_p R_p) H_n'(k\alpha_p R_{p-1}))^{-1} \tag{1.14}$$

$$\Gamma_n^p = [\alpha_p(J_n(k\alpha_p R_p)/J_n'(k\alpha_p R_p)) - \alpha_{p+1}(H_n(k\alpha_{p+1} R_p)/H_n'(k\alpha_{p+1} R_p))] \tag{1.15}$$

$$S_n^p = [\alpha_p(H_n(k\alpha_p R_p)/H_n'(k\alpha_p R_p)) - \alpha_{p+1}(J_n(k\alpha_{p+1} R_p)/J_n'(k\alpha_{p+1} R_p))] \tag{1.16}$$

$$D_n^p = [\alpha_p(H_n(k\alpha_p R_p)/H_n'(k\alpha_p R_p)) - \alpha_{p+1}(H_n(k\alpha_{p+1} R_p)/H_n'(k\alpha_{p+1} R_p))] \tag{1.17}$$

$$G_n^p = [\alpha_p(J_n(k\alpha_p R_p)/J_n'(k\alpha_p R_p)) - \alpha_{p+1}(J_n(k\alpha_{p+1} R_p)/J_n'(k\alpha_{p+1} R_p))] \tag{1.18}$$

$$d_n + f_n' = a_n^M + b_n^M \tag{1.19}$$

$$f_n = i^n J_n(kR_M) \tag{1.20}$$

$$f_n' = i^n k J_n'(kR_M) \tag{1.21}$$

The dual series equation was obtained in the form:

$$\begin{cases} \sum_{n=-\infty}^{\infty} A_n e^{in\phi} = 0, |\phi| \leq \theta \\ \sum_{n=-\infty}^{\infty} (A_n W_n - iZA_n) e^{in\phi} = \sum_{n=-\infty}^{\infty} F_n e^{in\phi}, \theta \leq |\phi| \leq \pi \end{cases}$$

(1.22)

$$A_n = a_n^M [\alpha_M (J_n(k\alpha_M R_M)/J_n'(k\alpha_M R_M)) - (H_n(kR_M)/H_n'(kR_M))]$$

-f$_n$ + b_n^M[α_M($H_n(k\alpha_M R_M)/H_n'(k\alpha_M R_M)$)
-(H$_n(kR_M)/H_n'(kR_M)$)] + $f_n'(H_n(kR_M)/H_n'(kR_M))$(1.23)

$$F_n = [i^n J_n'(kR_M)(H_n(kR_M)/H_n'(kR_M)) - i^n J_n(kR_M)]W_n \tag{1.24}$$

$$W_n = B_1|n| + o(|n|^{-1}) \tag{1.25}$$

$$B_1 = [kR_M(\varepsilon_M + \varepsilon_{M+1})]^{-1} \tag{1.26}$$

A dual series equation of this form enables the use of the method of analytical regularization for Riemann-Hilbert problem, transforming the problem into an infinite system of algebraic equations:

$$A_m = \sum_{n=-\infty}^{+\infty} [(|n| - B_1^{-1} W_n + iB_1^{-1} Z)A_n + B_1^{-1} F_n] T_{nm}(\theta) \tag{1.27}$$

where T_{nm} could be represented as in [26]:

$$T_{nm}(\theta) = (-1)^{m+n}[P_m(u)P_{n-1}(u) - P_{m-1}(u)P_n(u)]/2(m-n),\ m \neq n \tag{1.28}$$

$$T_{00}(\theta) = -ln\frac{(1+cos\theta)}{2} \tag{1.29}$$

$$T_{mm}(\theta) = \frac{1}{2|m|}[1 + \sum_{s=1}^{|m|} t_s(u)P_{s-1}(u)],\ m \neq 0 \tag{1.30}$$

where $t_0 = 1$, and $t_s(u) = P_s(u) - 2uP_{s-1}(u) + P_{s-2}(u)$.

Using [26], it can be shown that equation 1.27 represents a second-kind Fredholm matrix equation in the space of numerical sequences l_2. This indicates that equation 1.27 can be solved in the l_2 space for all real values of the wave number k (as purely real eigenvalues of k are prohibited by the Poynting theorem). Furthermore, the Fredholm nature of equation 1.27 ensures that solutions to truncated analogs of this equation converge to the exact solution of the infinite equation as the truncation order increases, i.e., as $N \longrightarrow \infty$, by the l_2 norm. This implies that for a limited number of components (within a specific truncation order), the solution will be approximate. However, as N grows large enough, it will approach the exact solution.

Therefore, based on these considerations, it can be confirmed that equation 1.27 is equivalent to the original boundary value problem (i)-(v).

1.2. Case of a point source

An additional important task is the investigation of waves excited by point sources.

By substituting the point source—i.e., replacing formula 1.6 with a formula in the following form:

$$H_z^{inc} = H_0^1(k|\vec{r} - \vec{r_s}|) \tag{1.31}$$

is emitted by the magnetic line current, placed at the point $\vec{r_s}$.

We arrive at a similar system to (1.22), where the function F takes the form

$$F_n = [f_n'(H_n(kR_M)/H_n'(kR_M)) - f_n]W_n \tag{1.32}$$

.

Using Graf's formula we obtained $f_n = J_n(kr_s)H_n(kr)$, $r_s < r$ and $f_n = J_n(kr)H_n(kr_s)$, $r_s > r$.

Chapter 2

Numerical results

The computational error is expressed as a function of the truncation number, N, in the following form:

$$e_{ACS}(N) = |S_{ACS}(N) - S_{ACS}(N_{max})|/S_{ACS}(N_{max}) \tag{2.1}$$

where S_{ACS} denotes the absorption cross-section. This parameter indicates the power lost in the graphene strip of the scatterer and can be determined from the Optical Theorem as shown below

$$S_{ACS}(N) = -(4/k)ReD_H(\phi_0, N) - S_{TSCS}(N) \tag{2.2}$$

where the far-field angular scattering pattern is expressed as:

$$D_H(\phi, N) = \sum_{n=-N}^{+N} d_n(-i)^n(H_n')^{-1}e^{in\phi} \tag{2.3}$$

and the total scattering cross-section is given by the following expression:

$$S_{TSCS}(N) = (4/k)\sum_{n=-N}^{+N} |d_n|^2|H_n'|^{-2} \tag{2.4}$$

The lens-with-strip focusing ability (FA) is defined as the field magnitude from inside, i.e., at:"

$$FA = |\sum_{n=-N}^{+N} [a_n^M \frac{\alpha_M J_n(k_M R_M)}{J_n'(k_M R_M)} + b_n^M \frac{\alpha_M H_n(k_M R_M)}{H_n'(k_M R_M)}]e^{in\phi_0}| \tag{2.5}$$

The panels shown in Figures 2.1 to the Figures 2.11 have been previously published and are discussed in detail in [1].

For the illustration of the focusing abilities, we constructed reliefs that depend on frequency and coordinates.

In Figures 2.2 to 2.4, the red spots correspond to the frequencies at which plasmon modes are excited on the graphene strip.

In Figure 2.5, to demonstrate the influence of the number of lens layers, we plotted the curves. It is clearly visible that starting from five layers, adding additional layers has a minimal effect on the frequency deviations and the maximum focusing values

Figures 2.6 and 2.7 shows the amplitude near-field patterns and their zooms at the frequency of the first (P1) and third (P3) plasmon mode resonance.

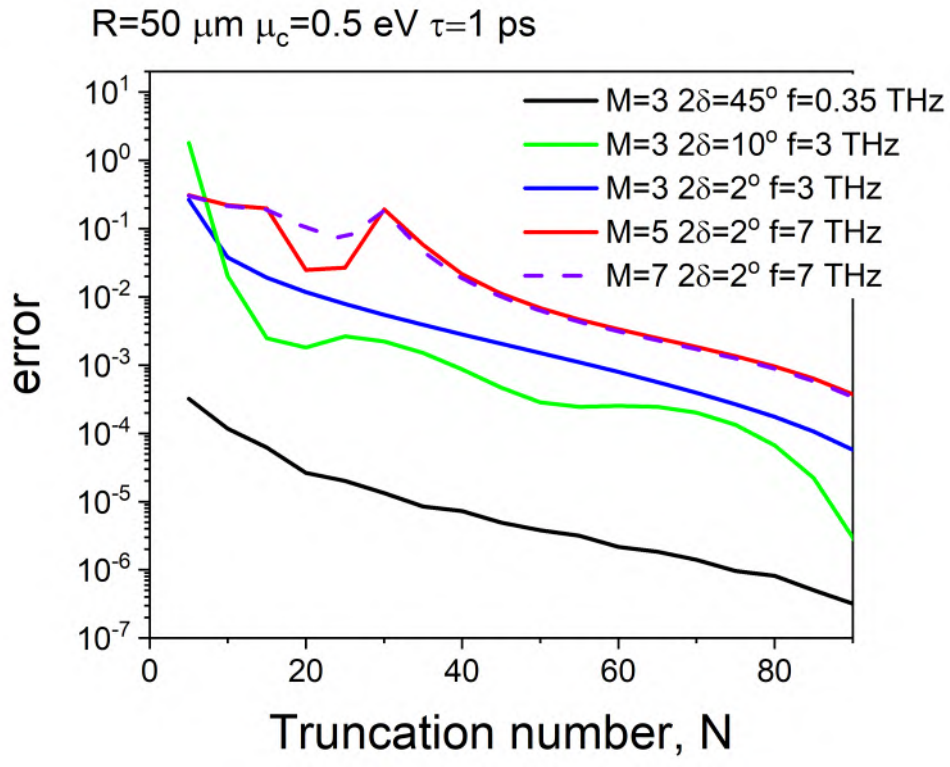

Figure 2.1: The computational error described in equation 2.1 plotted as a function of the matrix truncation number, for $N_{max} = 100$

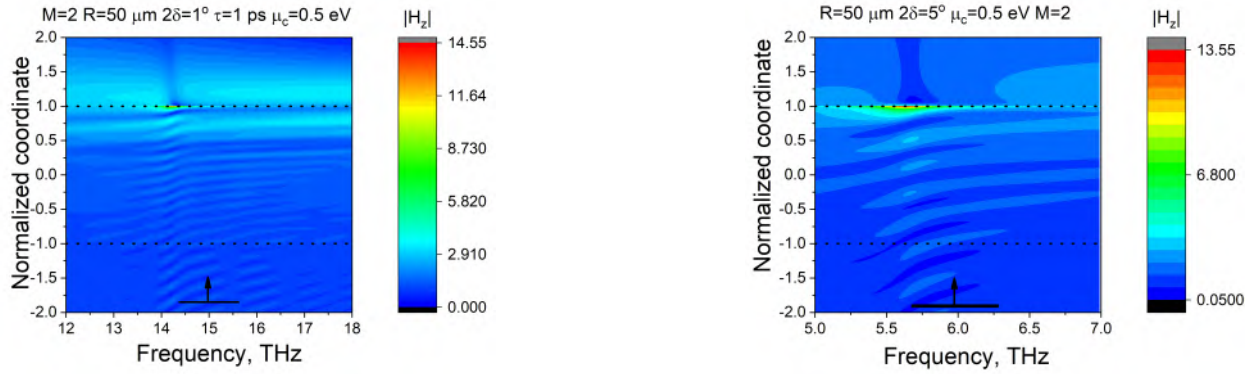

(a) (b)

Figure 2.2: The near-field magnitude along the x-axis for graphene strip angular widths of $2\delta = 1^\circ$ (a) and $2\delta = 5^\circ$ (b). The plane wave propagates along the symmetry line of the Luneburg lens, which has $M = 2$ layers.

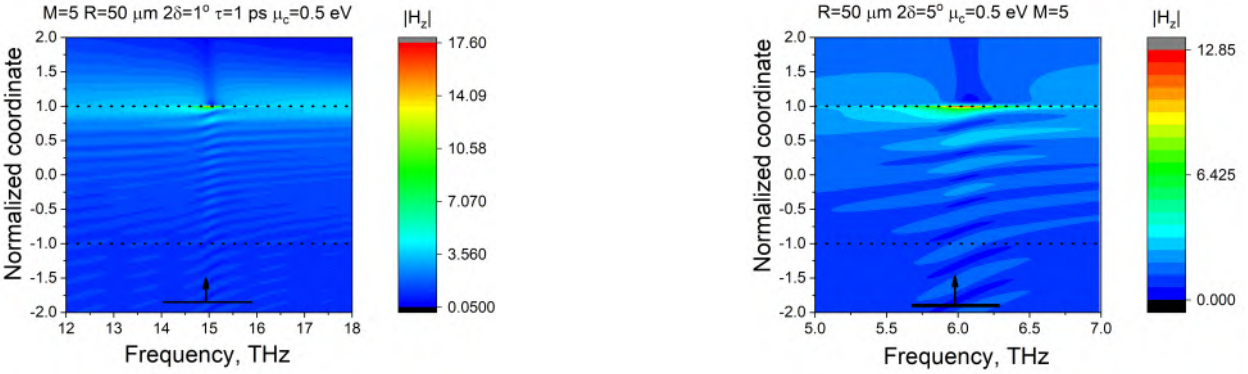

(a) (b)

Figure 2.3: The near-field magnitude along the x-axis for graphene strip angular widths of $2\delta = 1^\circ$ (a) and $2\delta = 5^\circ$ (b). The plane wave propagates along the symmetry line of the Luneburg lens, which has $M = 5$ layers.

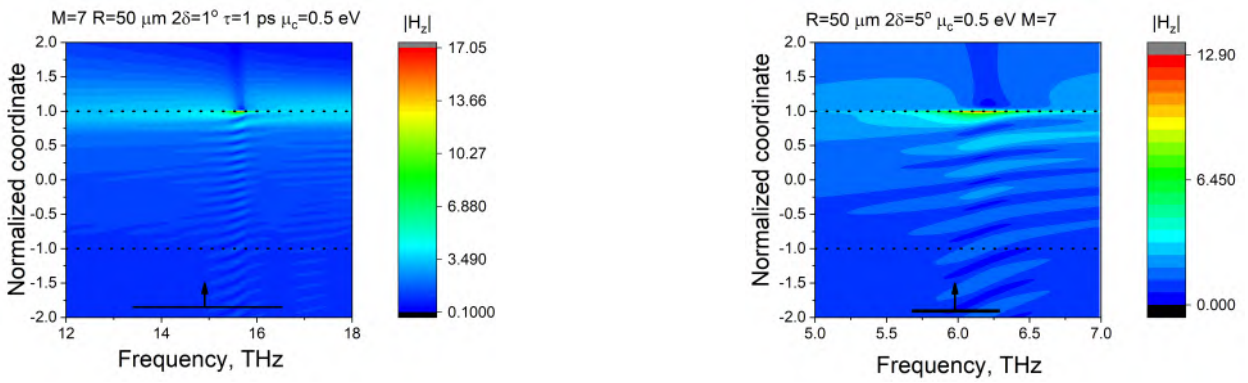

(a) (b)

Figure 2.4: The near-field magnitude along the x-axis for graphene strip angular widths of $2\delta = 1^\circ$ (a) and $2\delta = 5^\circ$ (b). The plane wave propagates along the symmetry line of the Luneburg lens, which has $M = 7$ layers.

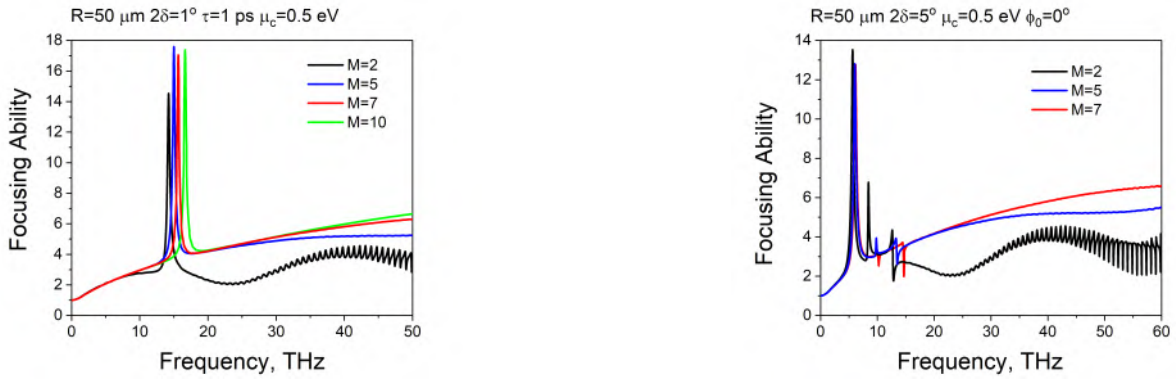

(a) (b)

Figure 2.5: Focusing ability versus frequency for graphene strip angular widths of $2\delta = 1^\circ$ (a) and $2\delta = 5^\circ$ (b), under symmetric plane-wave excitation, with a matrix truncation order of $N = 160$

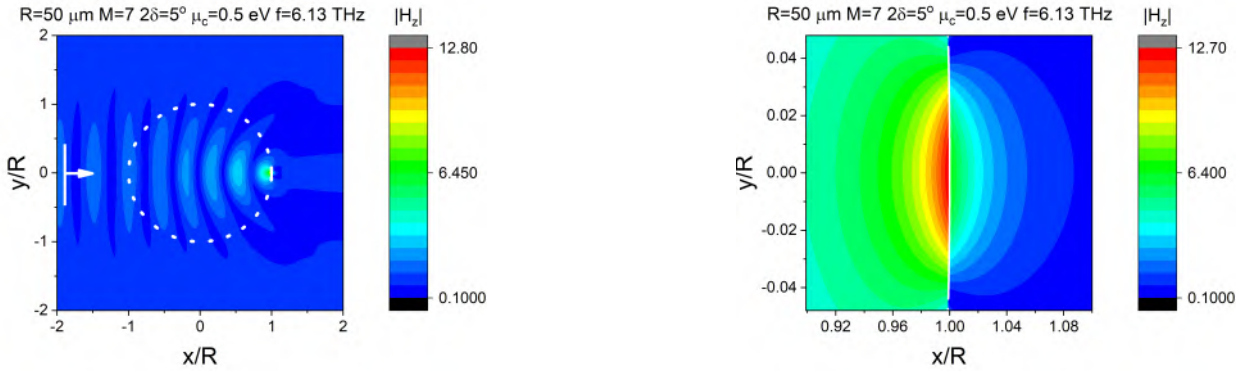

(a) (b)

Figure 2.6: The amplitude near-field patterns (a) and their zooms (b) at the frequency of the first plasmon mode (P1) resonance, with a matrix truncation order of $N = 160$ and a graphene strip angular width of $2\delta = 5°$.

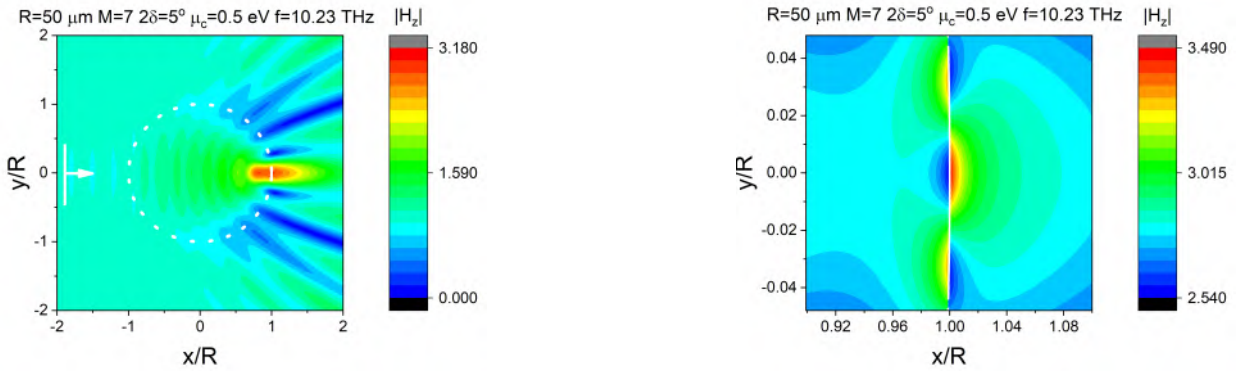

(a) (b)

Figure 2.7: The amplitude near-field patterns (a) and their zooms (b) at the frequency of the third plasmon mode (P3) resonance, with a matrix truncation order of $N = 160$ and a graphene strip angular width of $2\delta = 5°$.

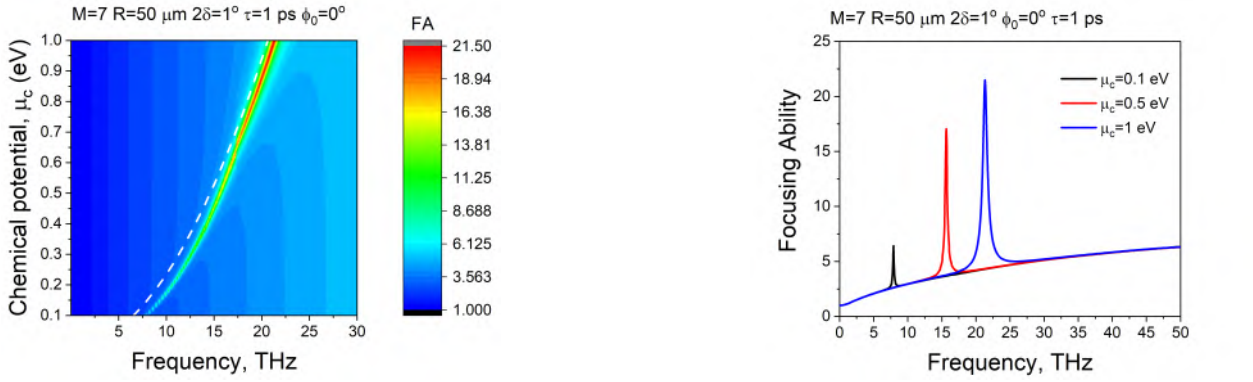

(a) (b)

Figure 2.8: The color map of focusing ability versus frequency and chemical potential (a), and the plots of focusing ability versus frequency (b) for a graphene strip with an angular width of $2\delta = 5^\circ$ under symmetric plane-wave excitation, $\phi_0 = 0$. The white dashed line corresponds to the analytical formula of the first plasmon mode [1].

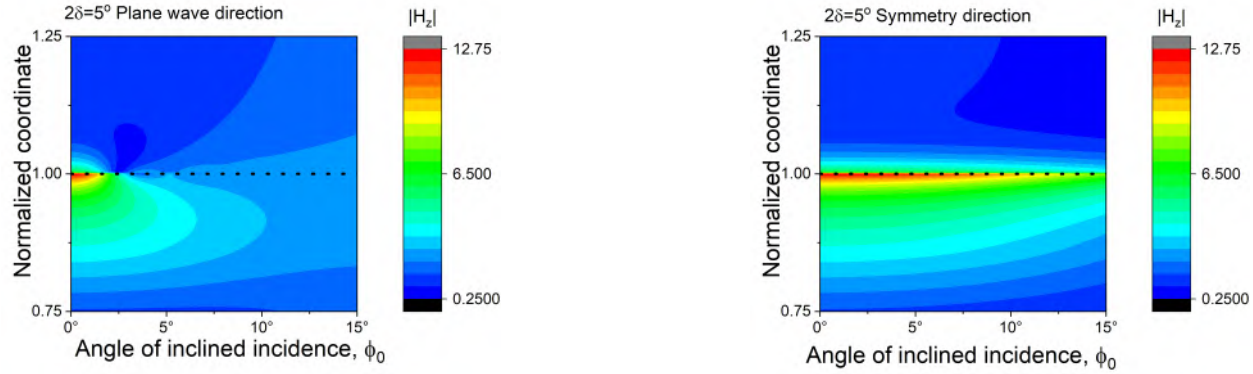

(a) (b)

Figure 2.9: The near-field magnitude along the x-axis for a graphene strip with an angular width of $2\delta = 5^\circ$ versus the plane-wave incidence angle, ϕ_0, for a number of layers $M = 7$.

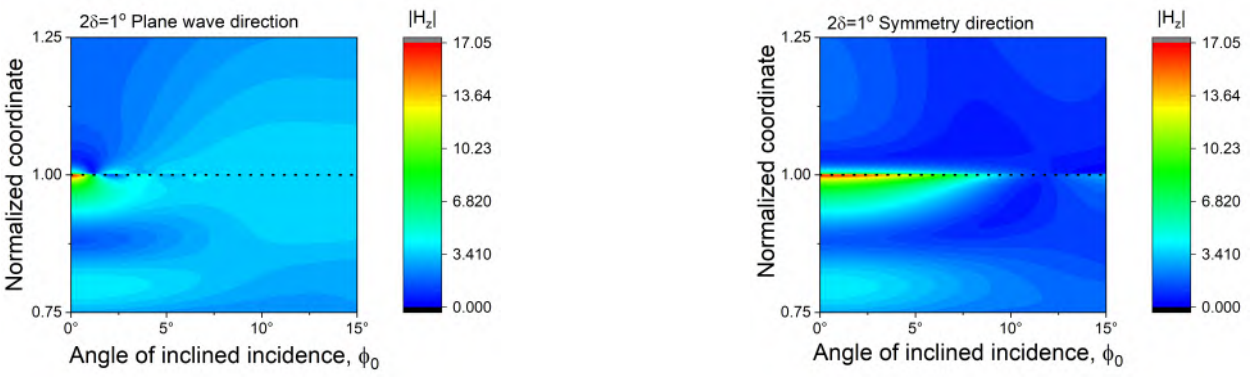

(a) (b)

Figure 2.10: The near-field magnitude along the x-axis for a graphene strip with an angular width of $2\delta = 1^\circ$ versus the plane-wave incidence angle, ϕ_0, for a number of layers $M = 7$.

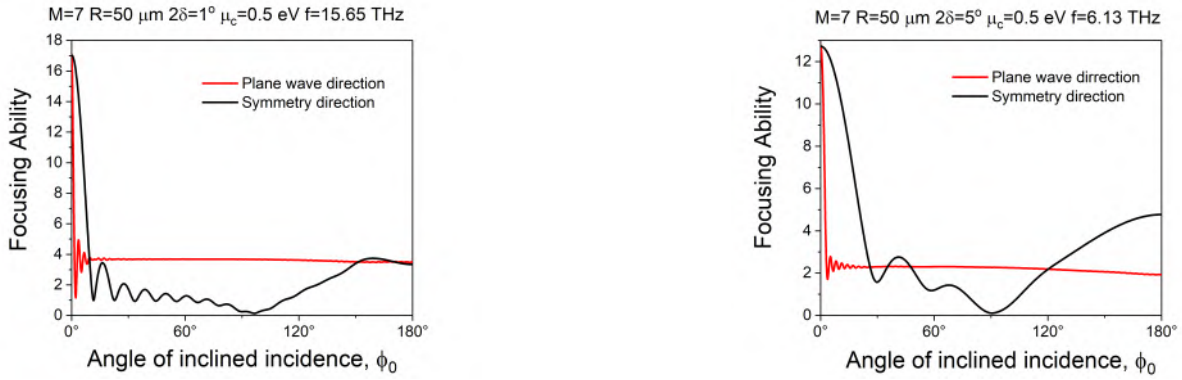

(a) (b)

Figure 2.11: Focusing ability versus plane wave incidence angle for graphene strip angular widths of $2\delta = 1^\circ$ (a) and $2\delta = 5^\circ$ (b), at the frequency corresponding to the first plasmon mode (P1) resonance of the strip.

Chapter 3
Numerical results for the case of a point source

In the case of a point source how it was mentioned before, it is necessary to analyze the radiation power and directivity.

Further we compute and discuss several characteristics, which depend on the frequency and size of the graphene strip. In the far zone, the total field is a cylindrical wave

$$H_z(\vec{r}) = \Phi(\phi)(1/\pi kr)^{1/2} e^{ikr} \tag{3.1}$$

with the following parts of the angular radiation pattern,

$$\Phi(\phi) = \Phi_{in}(\phi) + \Phi_{sc}(\phi), \Phi_{in}(\phi) = e^{ikr_0 \cos(\phi - \phi_0)} \tag{3.2}$$

$$\Phi_{sc}(\phi) = \sum_{n=-\infty}^{+\infty} (-i)^n d_n e^{in\phi} / H_n'(kR_M) \tag{3.3}$$

The total radiation power is, by definition,

$$P_{rad} = (\pi k Z_0)^{-1} \int_0^{2\pi} |\Phi(\phi)|^2 d\phi \tag{3.4}$$

After algebraic transformations the integral is reduced to the sum over the found unknown coefficients d_n. Note that the radiated power equals to the radiation conductance times the square of the magnetic current in the line source.

The absorption power consists of two parts, corresponding to the power,

absorbed in the lossy graphene strip,

$$P_{abs}^{grph} = ReZR \int_{-\delta}^{+\delta} |v(\phi)|^2 d\phi \tag{3.5}$$

where $v(\phi)$ is the current on the graphene strip.

And the power absorbed in a lossy lens layer, if it is present. If the lens is assumed lossless, the radiation efficiency is the ratio,

$$\eta = P_{rad}/(P_{rad} + P_{abs}^{grph}) \tag{3.6}$$

In our calculations, we use the radiation power of the magnetic line in the free space, $P_0 = 2(kZ_0)^{-1}$, for the normalization of radiated power of the line-fed layered LL.

Now we demonstrate the results, calculated for two angular sizes of graphene strip and for different numbers of layered lens layers. As can be seen from the emission and absorption power plots, there is a sharp increase in the powers when the source frequency approaches the real parts of the natural frequencies of the strip plasmon modes. Besides, the black curves in Fig. 3(a) show periodic peaks above 12 THz each time the frequency coincides with the natural frequency of a high-Q WGM.

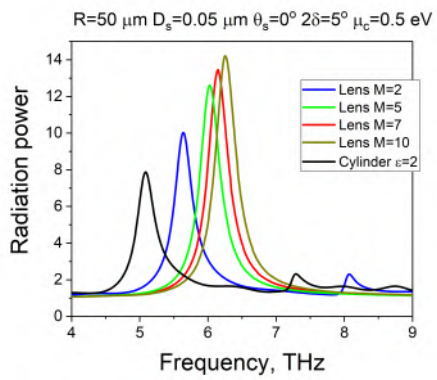

(a)

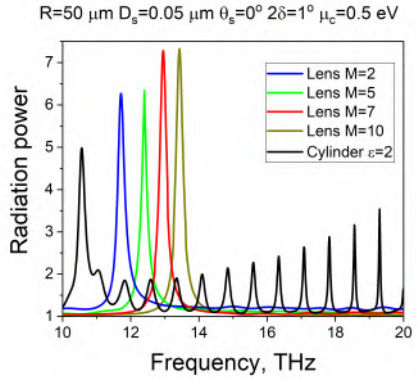

(b)

Figure 3.1: Spectra of normalized radiation versus the frequency for different numbers of layers. Lens has radius $R_M = 50\mu m$. Graphene strip angular width is $2\delta = 5^o$ (a) and $2\delta = 1^o$ (b). The source is on the x-axis at the distance $Ds = 50nm$ from the lens.

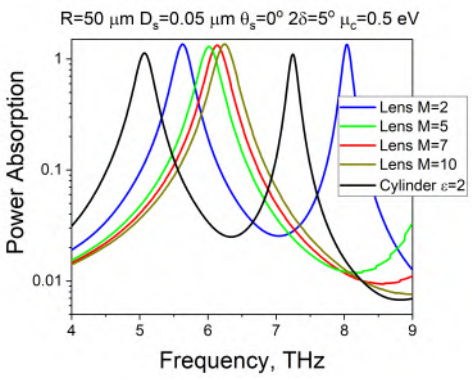

(a)

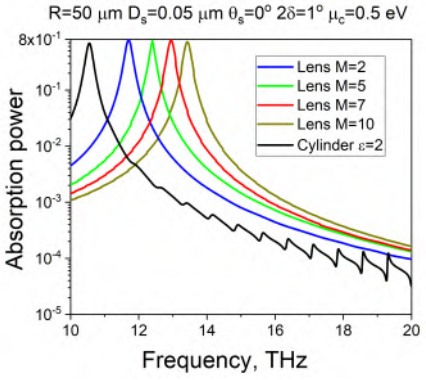

(b)

Figure 3.2: Absorption resistances (or powers) versus the frequency for different numbers of layers. Lens has radius $R_M = 50\mu m$. Graphene strip angular width is $2\delta = 5^o$ (a) and $2\delta = 1^o$ (b). The source is on the x-axis at the distance $D_s = 50nm$ from the lens.

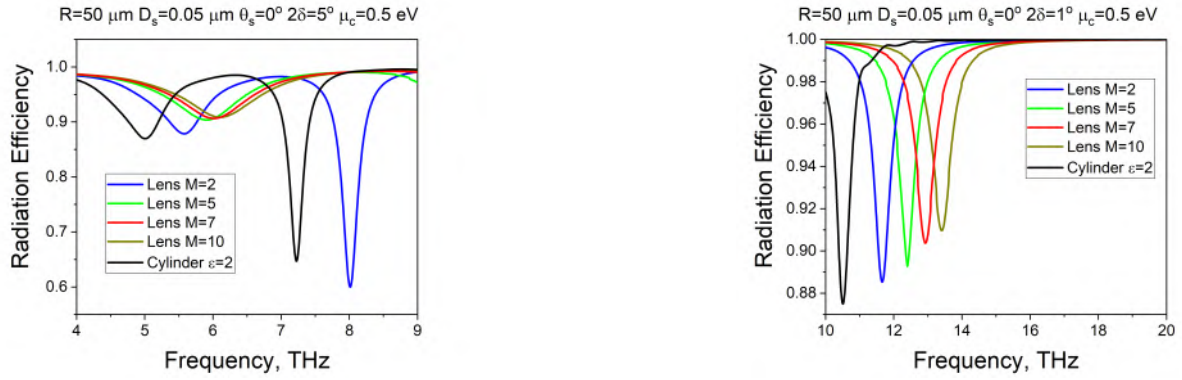

(a) (b)

Figure 3.3: Radiation efficiency versus the frequency for different numbers of layers. Lens has radius $R_M = 50\mu m$. Graphene strip angular width is $2\delta = 5^o$ (a) and $2\delta = 1^o$ (b). The source is on the x-axis at the distance $D_s = 50nm$ from the lens.

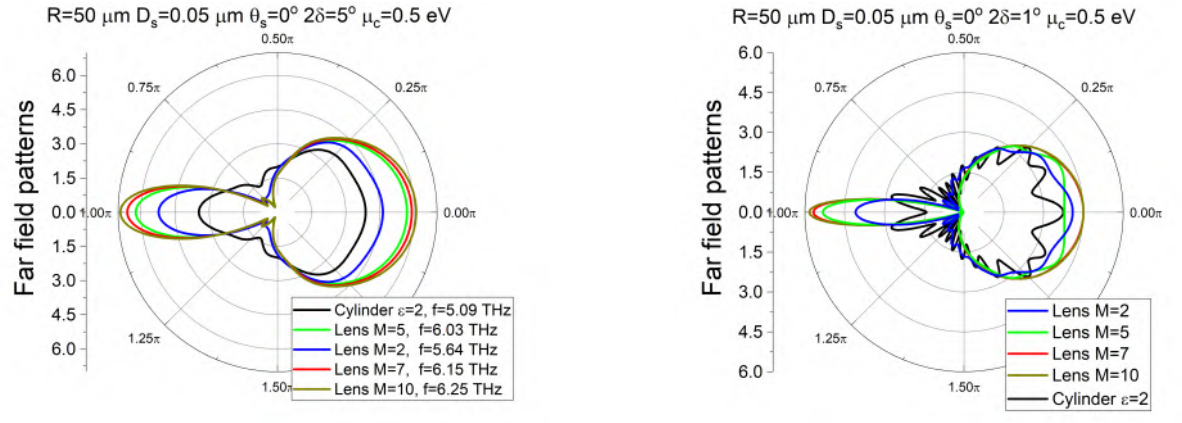

(a) (b)

Figure 3.4: In-resonance normalized far field emission patterns corresponding to Fig.3.1 and Fig.3.2. Graphene strip angular width is $2\delta = 5^o$ (a) and $2\delta = 1^o$ (b).

Conclusions

In the course of this work, materials related to the scattering and focusing properties of the Luneburg lens were analyzed and examined. The physical properties of graphene structures were explored. A double system of equations was derived using the boundary problem method, which, through the application of the method of analytical regularization to Riemann-Hilbert problems, was reduced to an infinite system of algebraic equations. A system of Fredholm second kind was obtained. A program was developed based on the system after truncation. Various characteristics, including focusing properties, absorption characteristics, and scattering characteristics were computed. One of the key aspects of the work was demonstrating the convergence of the method. The results obtained in this Master Thesis can be used for modeling antenna structures based on the Luneburg lens and graphene elements.

Appendix 1

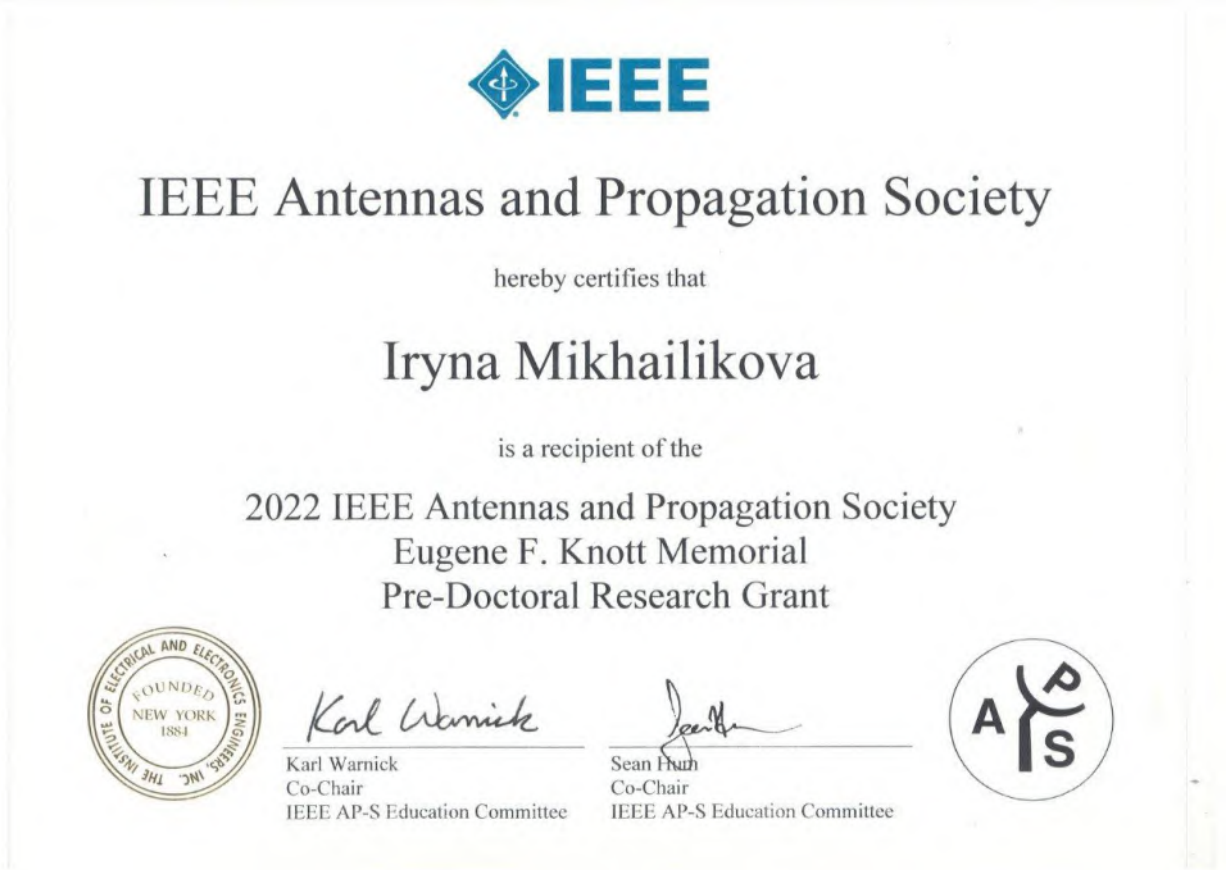

IEEE

IEEE Antennas and Propagation Society

hereby certifies that

Iryna Mikhailikova

is a recipient of the

2022 IEEE Antennas and Propagation Society
Eugene F. Knott Memorial
Pre-Doctoral Research Grant

THE INSTITUTE OF ELECTRICAL AND ELECTRONICS ENGINEERS, INC. FOUNDED NEW YORK 1884

Karl Warnick
Co-Chair
IEEE AP-S Education Committee

Sean Hum
Co-Chair
IEEE AP-S Education Committee

AP S

Appendix 2

IEEE Photonics Society

2024 Graduate Student Scholarship

presented to

Iryna Mikhailikova

V.N. Karazin Kharkiv National University

IEEE

Perry Shum —Photonics Society President

IEEE photonics Society

Bibliography

[1] I. O. Mikhailikova, D. M. Natarov, S. V. Dukhopelnykov, R. Sauleu, M. Lucido, and O. I. Nosich, "Tunable enhancement of cylindrical Luneburg lens focusing ability with the aid of conformal graphene strip," Optics Express, vol. 32, no.23, 2024, pp. 41726-41740.

[2] I.O. Mikhailikova, S.V. Dukhopelnykov, "2-D scattering and absorption of E-polarized plane wave by a circular dielectric wire with partial graphene cover," Proc. Europ. Microw. Conf. (EuMC-2022), Milan, 2022, pp. 290-3.

[3] I.O. Mikhailikova, S.V. Dukhopelnykov, R. Sauleau, "Non-plasmon resonances in the E-polarized plane wave scattering and absorption by a circular dielectric wire with partial graphene cover," Proc. Int. Conf. Electronics and Nanotechnology (ELNANO-2022), Kyiv, 2022, pp. 160-163.

[4] I.O. Mikhailikova, S.V. Dukhopelnykov, "Elementary electric dipole excitation of graphene spherical disk," Proc. Int. Conf. Ukrainian Microwave Week (UkrMW-2022), Kharkiv, 2022, pp. 388–391.

[5] I.O. Mikhailikova, S.V. Dukhopelnykov, "MAR algorithm for cylindrical Luneburg lens equipped with conformal graphene strip," European Conf. Antennas Propagation (EuCAP-2023), Florence, 2023, pp. 1-4.

[6] I.O. Mikhailikova, S.V. Dukhopelnykov, "Cylindrical Luneburg lens equipped with conformal graphene strip as efficient THz absorber,"

Proc. European Microwave Conf. (EuMC-2023), Berlin, 2023, pp. 484-487.

[7] I.O. Mikhailikova, S. Dukhopelnykov, M. Lucido, "Influence of the incidence angle on the focusing of Luneburg lens partially covered with graphene," Proc. European Conf. Antennas Propagat. (EuCAP-2024), Glasgow, 2024.

[8] I.O. Mikhailikova, S. Dukhopelnykov, "Improvement of 2-D Luneburg lens focusing ability with the aid of conformal graphene strip," Int. Symp. IEEE Antennas and Propagation (AP-S 2024), Florence, 2024.

[9] I.O. Mikhailikova, S. Dukhopelnykov, "Luneburg Lens Focusing Improvement with the Aid of Graphene Strip Tuned to Plasmon Resonance," Proc. European Microwave Conf. (EuMC-2024), Paris, 2024, pp. 1016-1019

[10] R. K. Luneburg, The Mathematical Theory of Optics. Providence, Brown Univ. Press, 1941.

[11] A. Parfitt, J. Graeme, J. Kot, and P. Hall, "A case for the Luneburg lens as the antenna elements for the square-kilometre array radio telescope," Radio Sci. Bulletin, no 293, pp. 32-37, 2000.

[12] A. V. Boriskin and A. I. Nosich, "Whispering-gallery and Luneburg lens effects in a beam-fed circularly-layered dielectric cylinder," IEEE Trans. Antennas Propagat., vol. 50, no 9, pp. 1245-1249, 2002.

[13] Z. Sipus, D. Bojanjac, and T. Komljenovic, "Electromagnetic modeling of spherically stratified lenses illuminated by arbitrary sources," ," IEEE Trans. Antennas Propagat., vol. 60, no 4, pp. 1837-1842, 2015.

[14] P. Kadera, A. Jiménez-Sáez, and J. Lacik, "Sub-THz Luneburg lens enabled wide-angle frequency-coded identification tag for passive indoor self-localization," Int. J. Microwave Wireless Technol., vol. 15, no 1, pp. 59-73, 2022.

[15] S.V. Dukhopelnykov, et al, "Circular dielectric rod with conformal strip of graphene as tunable terahertz antenna: interplay of inverse electromagnetic jet, whispering gallery and plasmon effects," IEEE J. Sel. Top. Quant. Electron., vol. 27, no 1, art. no 4600908, 2021.

[16] G. W. Hanson, "Dyadic Green's functions and guided surface waves for a surface conductivity model of graphene," J. Appl. Phys., vol. 103, pp. 064302, 2008.

[17] Z. Ullah, et al., "A review on the development of tunable graphene nanoantennas for terahertz optoelectronic and plasmonic applications," Sensors, vol. 20, no 5, art. no 1401, 2020.

[18] M. Lucido, M. V. Balaban, and A. I. Nosich, "Terahertz range plasmon and whispering gallery mode resonances in the plane wave scattering from thin microsize dielectric disk with graphene covers," Proc. Royal Society A, vol. 478, no 2262, art. no 20220126, 2022.

[19] F. O. Yevtushenko, et al., "Spoiling of tunability of on-substrate graphene strip grating due to lattice-mode-induced transparency," RSC Advances, vol. 12, no 8, pp. 4589–4594, 2022.

[20] S. V. Dukhopelnykov, R. Sauleau, M. Garcia-Vigueras, and A. I. Nosich, "Combined plasmon-resonance and photonic-jet effect in the THz wave scattering by dielectric rod decorated with graphene strip," J. Applied Physics, vol. 126, no 2, art. no 023104, 2019.

[21] A. Heifetz, et al., "Photonic nanojets," J. Comput. Theoretical Nanoscience, vol. 6, no. 9, pp. 1979–1992, 2009.

[22] S. V. Dukhopelnykov et al., "Integral equation analysis of terahertz backscattering from circular dielectric rod with partial graphene cover," IEEE J. Quant. Electron., vol. 56, no 6, art. no 8500208, 2020.

[23] Y. Jeyar, et al., "Electromagnetic scattering by a partially graphene-coated dielectric cylinder: efficient computation and multiple plasmonic resonances," Phys. Rev. E, vol. 107, art. no 025306, 2023.

[24] H. Sakurai, T. Hashidate, M. Ohki, K. Motojima, and S. Kozaki, "Electromagnetic scattering by the Luneberg lens with reflecting cap," IEEE Trans. Electromagn. Compat., vol. 40, no 2, pp. 94–96, 1998.

[25] N. Nikolic, J. S. Kot, and S. Vinogradov, "Scattering by a Luneburg lens partially covered by a metallic cap," J. Electromagn. Waves Applic., vol. 21, no 4, pp. 549–563, 2007.

[26] T. L. Zinenko and A. I. Nosich, "Plane wave scattering and absorption by flat gratings of impedance strips," IEEE Trans. Antennas Propagat., vol. 54, no 7, pp. 2088-2095, 2006.